Available online at www.sciencedirect.com

SCIENCE DIRECT®

Polyhedron 24 (2005) 267–279

POLYHEDRON

www.elsevier.com/locate/poly

The synthesis, spectroscopic characterisation, crystal and molecular structure of the [$ReCl_3(NO)(OPPh_3)(pyz)$] complex. DFT calculations for [$ReCl_3(NO)(OPPh_3)(pyz)$] and [$ReCl_3(NO)(OPPh_3)(PPh_3)$]

B. Machura [a,*], M. Jaworska [b], R. Kruszynski [c,1]

[a] *Department of Inorganic and Radiation Chemistry, Institute of Chemistry, University of Silesia, 9th Szkolna St., 40-006 Katowice, Poland*
[b] *Department of Theoretical Chemistry, Institute of Chemistry, University of Silesia, 9th Szkolna St., 40-006 Katowice, Poland*
[c] *Department of X-ray Crystallography and Crystal Chemistry, Institute of General and Ecological Chemistry,*
Lodz University of Technology, 116 Żeromski St., 90-924 Łódź, Poland

Received 8 September 2004; accepted 9 November 2004

Abstract

A new rhenium nitrosyl – [$ReCl_3(NO)(OPPh_3)(pyz)$] – has been obtained by two different routes: (i) in the substitution reaction of [$ReCl_3(NO)(OPPh_3)(PPh_3)$] with pyrazine, and (ii) in the nitrosylation reaction of [$ReOCl_3(PPh_3)_2$] by gaseous nitric oxide in the presence of an excess of pyrazine. The crystal, molecular and electronic structure of the [$ReCl_3(NO)(OPPh_3)(pyz)$] complex has been determined. The geometric parameters of [$ReCl_3(NO)(OPPh_3)(pyz)$] have been examined using the density functional theory (DFT) method. The UV–Vis spectrum of the pyrazine complex has been interpreted on the basis of the electronic transitions of [$ReCl_3(NO)(OPPh_3)(pyz)$] calculated with the time-dependent DFT method (TDDFT). The paper also includes the results of the DFT and TDDFT calculations for [$ReCl_3(NO)(OPPh_3)(PPh_3)$].

Keywords: Rhenium nitrosyl complexes; Pyrazine; X-ray structure; DFT and TDDFT calculations

---

1. Introduction

For many years nitrosyl compounds of transition metals have been the centre of interest of scientists both engaged in basic research and trying to employ these complexes as catalysts of polymerisation, oligomerisation, metathesis, epoxidation, oxidation and reduction [1–11].

One of the most important aspects of the research on nitrosyl complexes is determination of the bonding nature of NO to the metal center. Terminal NO ligands may adopt either linear or bent geometries. Although the bonding in the M–NO moiety is largely of covalent nature and the electron distribution is more or less evenly distributed in this group, the bonding of the M–NO unit is often described by assigning formal oxidation states to the metal centre and the nitrosyl ligand. In such an assignment nitric oxide can be coordinated as NO^+, NO or NO^-. The M–NO core can be also described using the $\{M(NO)_x\}^n$ formalism proposed by Enemark and Feltham, in which n is taken as the total number of electrons associated with the metal d and $\pi^*(NO)$ orbitals [1,3,9,11].

---

[*] Corresponding author. Tel.: +48322582441; fax: +48322599978.
E-mail addresses: bmachura@poczta.onet.pl (B. Machura), mj@tc3.ich.us.edu.pl (M. Jaworska), kruszyna@p.lodz.pl (R. Kruszynski).

[1] A holder of the Foundation for Polish Science (FNP) scholarship.

0277-5387/$ - see front matter © 2004 Elsevier Ltd. All rights reserved.
doi:10.1016/j.poly.2004.11.024

Due to the favourable nuclear properties of ^{186}Re and ^{188}Re nuclides in diagnostic nuclear medicine and applications in radioimmunotherapy [12,13], the chemistry of nitrosyl rhenium complexes arouses particular interest.

The papers [14–22] present the preparation, structural and spectroscopic characterisation of rhenium mononitrosyls with phosphine and arsine ligands in the coordination sphere.

Here we present the synthesis, crystal, molecular and electronic structure of a new rhenium nitrosyl with pyrazine (pyz) in the coordination sphere – [ReCl$_3$(NO)(OPPh$_3$)(pyz)] (**1**). The electronic structure of **1** has been determined on the basis of density functional theory (DFT) calculations. The spin-allowed doublet–doublet electronic transitions of [ReCl$_3$(NO)(OPPh$_3$)(pyz)] have been calculated with the time-dependent DFT (TDDFT) method, and the UV–Vis spectrum of the title complex has been discussed on this basis. For comparison, the paper includes also the results of the DFT and TDDFT calculations for [ReCl$_3$(NO)(OPPh$_3$)(PPh$_3$)] (**2**). The crystal, molecular structure and spectroscopic properties of **2** were presented in paper [17].

Recent calculations with the TDDFT method for open- and closed-shell 5d-metal complexes have supported the TDDFT method to be applicable for such systems giving good assignment of experimental spectra [23–29]. Some theoretical investigations have also been carried out on rhenium compounds. The electronic structures of nitrido, oxo, carbonyl and nitrile rhenium complexes, as well as their spectroscopic properties, bonding and reactivity have been theoretically studied at the HF, MP2, EHT and DFT levels of theory using various basis sets [30–37]. Gancheff et al. [32] have performed extended tests of the ability of the B3LYP method in the LANL2DZ basis set for rhenium compounds in a geometry optimisation and calculation of spectral properties. Although this is not a very extended basis set, its use with DFT has been shown to be sufficient for geometry optimisation and calculation of spectral properties. It gives good agreement with the experimental data and its use is especially justified in the case of large molecules.

2. Experimental

2.1. General procedure

The reactions were carried out under an argon atmosphere. All the reagents used for the syntheses of the complexes are commercially available and were used without further purification. [Re(NO)Cl$_3$(PPh$_3$)(OPPh$_3$)] and [ReOCl$_3$(PPh$_3$)$_2$] complexes were prepared according to the literature methods [17,38]. Gaseous NO, obtained in reaction (1)

$$2\mathrm{NaNO_2} + 3\mathrm{H_2SO_4} + \mathrm{FeSO_4} \rightarrow 2\mathrm{NO} + 2\mathrm{NaHSO_4} + \mathrm{Fe_2(SO_4)_3} + 2\mathrm{H_2O} \quad (1)$$

was purified by passing through washers with concentrated KOH solution and over solid NaOH.

The IR spectrum of **1** was recorded on a Nicolet Magna 560 spectrophotometer in the spectral range 4000–400 cm^{-1} with the sample in the form of a KBr pellet. The electronic spectrum of **1** was measured on a Lab Alliance UV–Vis 8500 spectrophotometer in the range 800–220 nm in deoxygenated dichloromethane solution. Magnetic susceptibility was measured at 296 K by the Faraday method. Elemental analyses (C, H, N) were performed on a Perkin–Elmer CHN-2400 analyzer.

2.2. Preparation of [ReCl$_3$(NO)(OPPh$_3$)(pyz)] (1)

2.2.1. Method A

[Re(NO)Cl$_3$(OPPh$_3$)(PPh$_3$)] (1 g, 1.15 mmol) and pyz (0.5 g, 0.62 mmol) in chloroform (100 cm^3) were refluxed for 12 h. The volume was condensed to 20 cm^3 and a dark green microcrystalline solid was formed by addition of 100 cm^3 of diethyl ether. The product was washed with EtOH and cold ether, and dried in vacuo (Yield: 40%).

2.2.2. Method B

NO was passed through a vigorously stirred and refluxing solution of [ReOCl$_3$(PPh$_3$)$_2$] (1.05 g, 1 mmol) and pyz (0.25 g, 3.1 mmol) in acetone (100 cm^3). The reaction was carried out for 4 h. The colour changed gradually from bright green to dark green. Then the resulting solution was evaporated to a volume of 10 cm^3. A green precipitate was formed by an addition of 40 cm^3 of EtOH and after 15 min it was filtered off. The product was washed with cold ether and dried in vacuo. Crystals suitable for X-ray investigation were obtained by recrystallisation from CHCl$_3$–EtOH (Yield: 70%).

IR (KBr, cm^{-1}) 3059 (w), 1762 (s), 1589 (m), 1484 (s), 1440 (s), 1416 (3), 1354 (w), 1316 (w), 1270 (w), 1163(m), 1122 (s), 1060 (s), 1027 (m), 1001 (m), 807 (m), 753 (s), 727 (s), 691 (s), 616 (w), 552 (s), 536 (s), 466(s). Calc. for C$_{21}$H$_{19}$N$_3$Br$_3$OAsRe: C, 38.80; H, 2.81; N, 6.1. Found: C, 38.92; H, 2.75; N, 6.15%.

2.3. Crystal structure determination and refinement

The X-ray intensity data of complex **1** were collected on a KM-4-CCD automatic diffractometer equipped with a CCD detector with 50 s exposure time and all reflections of the Ewald sphere were collected up to $\theta = 25°$. The unit cell parameters were determined from least-squares refinement of the setting angles of 9937 strongest reflections. Details concerning crystal data and refinement are given in Table 1. Lorentz, polarisation and numerical absorption corrections [39] were applied. The structure was solved by the Patterson method and subsequently completed by difference Fourier recycling. All the non-hydrogen atoms were refined anisotropically using the full-matrix, least-squares technique. The hydrogen atoms of the phenyl rings were treated as "riding" on their parent carbon atoms [d(C–H) = 0.96 Å] and assigned isotropic temperature factors equal to 1.2 times the value of the equivalent temperature factor of the parent carbon atom. SHELXS97 [40], SHELXL97 [41] and SHELXTL [42] programs were used for all the calculations. Atomic scattering factors were those incorporated in the computer programs.

2.4. Computational details

The GAUSSIAN03 program [43] was used in the calculations. The geometry optimisation was carried out with the DFT method with the use of the B3LYP functional [44,45]. The electronic spectra were calculated with the TDDFT method [46].

In the calculations, the LANL2DZ basis set [47] was used on the rhenium atom, 6-31G(d) on the chlorine, nitrogen, phosphorous, oxygen and carbon atoms and 6-31G basis on the hydrogen atoms.

Natural bond orbital (NBO) calculations were performed with the NBO code [48] included in GAUSSIAN03.

3. Results and discussion

3.1. Preparation

Two different routes have been employed for the preparation of **1**. The refluxing of $[ReCl_3(NO)(OPPh_3)(PPh_3)]$ with pyrazine (pyz) (Eq. (2)) in chloroform gives complex **1** in a moderate yield

$$[\mathrm{ReCl_3(NO)(OPPh_3)(PPh_3)}] + \mathrm{pyz} \rightarrow [\mathrm{ReCl_3(NO)(OPPh_3)(pyz)}] + \mathrm{PPh_3} \quad (2)$$

A much higher yield of **1** has been reported for the nitrosylation reaction of $[ReOCl_3(PPh_3)_2]$ by gaseous nitric oxide in the presence of an excess of pyrazine.

3.2. Crystal structure

A thermal ellipsoid plot of **1** is shown in Fig. 1. The rhenium atom of **1** is in a distorted octahedral

Table 1
Crystal data and structure refinement for $[ReCl_3(NO)(OPPh_3)(pyz)]$

Empirical formula	$C_{22}H_{19}Cl_3N_3O_2PRe$
Formula weight	680.92
Temperature (K)	293(2)
Wavelength (Å)	0.71073
Crystal system	orthorhombic
Space group	*Pbcn*
Unit cell dimensions	
a (Å)	29.2078(14)
b (Å)	10.2887(4)
c (Å)	16.6705(7)
Volume (Å^3)	5009.7(4)
Z	8
D_{calc} (Mg/m^3)	1.806
Absorption coefficient (mm^{-1})	5.259
F(0 0 0)	2632
Crystal size (mm)	0.041 × 0.180 × 0.194
θ Range for data collection	2.81–25.11
Index ranges	$-28 \leqslant h \leqslant 34$; $-2 \leqslant k \leqslant 12$; $-19 \leqslant l \leqslant 19$
Reflections collected	51 246
Independent reflections (R_{int})	4464 (0.0558)
Completeness to 2θ (%)	89.4
Maximum and minimum transmission	0.867 and 0.739
Data/restraints/parameters	4464/0/289
Goodness-of-fit on F^2	1.117
Final *R* indices [$I > 2\sigma(I)$]	$R_1 = 0.0311$; $wR_2 = 0.0473$
R indices (all data)	$R_1 = 0.0486$; $wR_2 = 0.0522$
Largest differential peak and hole (e Å^{-3})	0.918 and −0.660

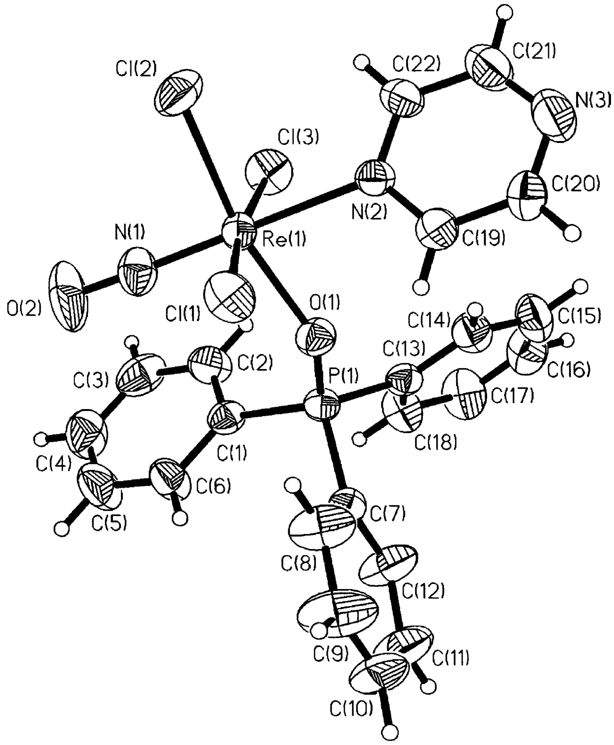

Fig. 1. Thermal ellipsoid plot of $[ReCl_3(NO)(OPPh_3)(pyz)]$ showing the atom numbering scheme (50% probability ellipsoids).

environment with the chloride ligands in *meridional* geometry and the linear N–O group *trans* to the pyrazine molecule and *cis* to the $OPPh_3$ ligand.

The molecules of **1** are linked via one C(12)–H(12)$\cdots$O2(x, $-y$, $z + 1/2$) intermolecular interaction, which according to Desiraju and Steiner [50] can be considered as a weak hydrogen bond with a D$\cdots$A distance equal to 3.317(6) Å and a D–H$\cdots$A angle of 143.9°. The weak intramolecular interaction C(19)–H(19)$\cdots$Cl(1) with a D$\cdots$A distance equal to 3.264(4) Å and a D–H$\cdots$A angle of 112.0° can also be treated as a weak hydrogen bond [49,50]. It provides additional conformational stabilisation of the $[ReCl_3(NO)(OPPh_3)(pyz)]$ molecule.

Table 1 presents the crystal data and structural refinement for complex **1**. The most important experimental bond lengths and angles of **1** are reported in Table 2. The Re–NO (1.740(4) Å) and N–O (1.184(4) Å) bond distances and the Re–N–O angle (176.0(6)°) indicate the nitrosonium character of the NO group. They are well compared with values previously found for other rhenium nitrosyls [14–22]. In comparison with the $[ReCl_3(NO)(OPPh_3)(PPh_3)]$ compound [1.747(5) and 1.165(8) Å] [25], an insignificant shortening of the Re–N distance and elongation of the N–O bond length can be noticed for complex **1**. The Re–$N_{pyrazine}$ distance is affected by the *trans* influence of the nitrosyl group and thus is longer than the Re–$N_{pyrazine}$ distances detected in $[ReO(OEt)Cl_2(pyz)_2]$ (2.152(16) and 2.103(16) Å) with a *trans* arrangement of the N-heterocyclic molecules [51]. The $OPPh_3$ ligand affects the Re–Cl(2) bond length and causes its shortening. A similar trend is observed for the $[ReCl_3(NO)(OPPh_3)_2]$ and $[ReBr_3(NO)(OPPh_3)_2]$ complexes with the halogen ligand in a *trans* position to the $OPPh_3$ molecule. The Re–$OPPh_3$ [2.058(2) Å] and P–O [1.521(3)] bond lengths in **1** are in good agreement with values found for $[ReCl_3(NO)(OPPh_3)_2]$ (Re–O = 2.055(6) Å, P–O = 1.493(6) Å) and $[ReBr_3(NO)(OPPh_3)_2]$ (Re–O = 2.048(4) Å, P–O = 1.505(4) Å) [18,21]. In complex **2**, the Re–$OPPh_3$ distance (2.103(5) Å) is affected by the nitrosyl group and thus is longer than the Re–$OPPh_3$ bond length in **1**.

Table 2
The experimental and optimised bond lengths (Å) and angles (°) for $[ReCl_3(NO)(OPPh_3)(pyz)]$

	Experimental	Optimised
Bond lengths		
Re(1)–N(1)	1.740(4)	1.758
Re(1)–N(2)	2.231(3)	2.245
Re(1)–Cl(1)	2.3656(11)	2.453
Re(1)–Cl(2)	2.3472(11)	2.409
Re(1)–Cl(3)	2.3734(11)	2.458
Re(1)–O(1)	2.058(2)	2.105
N(1)–O(2)	1.184(4)	1.171
P(1)–O(1)	1.521(3)	1.536
Bond angles		
N(1)–Re(1)–O(1)	98.49(14)	99.93
N(1)–Re(1)–N(2)	178.87(15)	177.50
O(1)–Re(1)–N(2)	81.31(11)	82.56
N(1)–Re(1)–Cl(2)	94.00(12)	91.70
O(1)–Re(1)–Cl(2)	167.47(8)	168.36
N(2)–Re(1)–Cl(2)	86.21(9)	85.81
N(1)–Re(1)–Cl(1)	94.03(12)	93.86
O(1)–Re(1)–Cl(1)	86.53(8)	86.09
N(2)–Re(1)–Cl(1)	87.07(9)	86.11
Cl(2)–Re(1)–Cl(1)	91.74(4)	92.66
N(1)–Re(1)–Cl(3)	93.72(12)	95.24
O(1)–Re(1)–Cl(3)	89.52(8)	86.89
N(2)–Re(1)–Cl(3)	85.17(9)	85.04
Cl(2)–Re(1)–Cl(3)	90.55(4)	92.59
Cl(1)–Re(1)–Cl(3)	171.75(4)	169.35
P(1)–O(1)–Re(1)	142.36(16)	141.72
O(2)–N(1)–Re(1)	178.2(3)	176.34

3.3. Infrared data and magnetochemical measurements of complex *1*

The IR spectrum of **1** exhibits a strong band at 1762 cm^{-1}, assignable to ν(NO). The value of ν(NO) corresponds to the linear NO range of Haymore and Ibers [52]. In the IR spectrum of complex **2**, the strong band corresponding to the stretching vibration of the nitrosyl group appears at 1745 cm^{-1}.

The sharp absorption band at 1598 cm^{-1} in the spectrum of **1** is typical of mono-coordinated diaza ligands [53]. The strong bands at 1163 and 1122 cm^{-1} confirm the presence of the coordinated $OPPh_3$ molecule.

The complex **1** is a paramagnetic compound with a room temperature magnetic moment of 1.8 BM, corresponding to one unpaired electron.

3.4. Optimised geometries of *1* and *2*

The geometries of **1** and **2** were optimised in a doublet state by the DFT method with the B3LYP functional. The doublet state agrees well with the experimental values of the effective magnetic moment for complexes **1** and **2**. The geometric parameters of **1** and **2** optimised by the DFT method are gathered in Tables 2 and 3, respectively. For comparison, the experimental bonds and bond angles of **2** are also included in Table 3. The structure and atomic numbering scheme of the complex **2** are shown in Fig. 2. The optimised geometries of **1** and **2** are in good agreement with the experimental ones, and the general trends observed in the experimental data are well reproduced in the calculations.

3.5. Charge distribution and spin densities of *1* and *2*

Table 4 presents the atomic charges from the natural population analysis (NPA) and spin densities for **1** and **2**. For both complexes the calculated charges on the rhenium atoms are considerably lower than the formal

Table 3
The experimental and optimised bond lengths (Å) and angles (°) for $[ReCl_3(NO)(OPPh_3)(PPh_3)]$

	Experimental	Optimised
Bond lengths		
Re(1)–N(1)	1.747(5)	1.751
Re(1)–P(2)	2.5288(18)	2.589
Re(1)–Cl(1)	2.3579(18)	2.425
Re(1)–Cl(2)	2.377(2)	2.453
Re(1)–Cl(3)	2.3502(18)	2.453
Re(1)–O(1)	2.103(5)	2.149
N(1)–O(2)	1.165(8)	1.172
P(1)–O(1)	1.506(5)	1.530
Bond angles		
N(1)–Re(1)–O(1)	176.6(2)	177.66
N(1)–Re(1)–Cl(3)	93.3(2)	94.87
O(1)–Re(1)–Cl(3)	90.05(15)	87.33
N(1)–Re(1)–Cl(1)	91.9(2)	93.17
O(1)–Re(1)–Cl(1)	84.77(15)	84.68
Cl(3)–Re(1)–Cl(1)	174.26(6)	171.18
N(1)–Re(1)–Cl(2)	93.5(2)	91.87
O(1)–Re(1)–Cl(2)	85.74(14)	87.32
Cl(2)–Re(1)–Cl(3)	90.76(8)	90.33
Cl(3)–Re(1)–Cl(1)	91.32(8)	90.33
N(1)–Re(1)–P(2)	93.0(2)	91.44
O(1)–Re(1)–P(2)	87.98(14)	89.53
Cl(3)–Re(1)–P(2)	85.18(7)	85.25
Cl(1)–Re(1)–P(2)	92.14(6)	90.95
Cl(2)–Re(1)–P(2)	171.75(4)	174.69
P(1)–O(1)–Re(1)	150.2(3)	148.76
O(2)–N(1)–Re(1)	176.0(6)	176.63

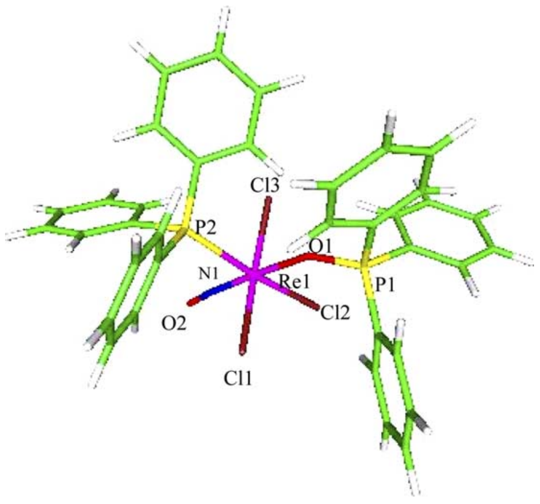

Fig. 2. Atomic numbering scheme of $[ReCl_3(NO)(OPPh_3)(PPh_3)]$.

Table 4
Atomic charges from the natural population analysis (NPA) and spin densities of **1** and **2**

Atom	1		2	
	Atomic charge	Spin density	Atomic charge	Spin density
Re(1)	0.830	1.079	0.593	1.034
Cl(1)	−0.453	0.036	−0.402	0.080
Cl(2)	−0.380	0.066	−0.441	0.054
Cl(3)	−0.466	0.033	−0.430	0.061
N(1)	0.254	−0.125	0.255	−0.112
O(2)	−0.225	−0.105	−0.235	−0.092
O(1)	−1.097	0.0144	−1.123	−0.001
P(1)	2.339	0.002	2.338	−0.000
N(2)	−0.479	−0.009		
N(3)	−0.400	0.001		
P(2)			1.385	−0.031

charge of +2. This is the result of charge donation from Cl^- ions, the charges on the chloride ligands are significantly smaller than −1. The rhenium atom of **2** is less positive than the Re atom of **1**. It results from the presence of triphenylphosphine in the coordination sphere of **2**. The PPh_3 molecule acts as a strong σ-donor; there is a large positive charge on the phosphorus atom of the coordinated triphenylphosphine in complex **2**. The oxygen atoms of the $OPPh_3$ ligands in **1** and **2** are negatively charged. The calculated charges on the nitrogen atoms of the nitrosyl groups are positive, whereas the oxygen atoms are negatively charged. The total charges on the NO groups are positive, being 0.029 and 0.020 for **1** and **2**, respectively.

For both complexes, there are positive spin densities of about 1 on the rhenium atoms and small negative spin densities of about −0.1 on the nitrogen and oxygen atoms of the nitrosyl ligands. The spin densities on the donor atoms of the other ligands are below 0.1 for complexes **1** and **2**.

3.6. Electronic structure

The energies and characters of several highest occupied and lowest unoccupied molecular orbitals of **1** and **2** are presented in Tables 5 and 6, respectively. Most of the MOs of **1** and **2** have complicated characters. The percent participation of atomic orbitals in the selected HOMO and LUMO orbitals for **1** and **2** are shown in Tables 5 and 6, respectively.

3.7. $[ReCl_3(NO)(OPPh_3)(pyz)]$ (*1*)

In the molecular orbital approach, the bonding of NO to a metal is considered to be made up of two components. The first involves donation of electron density from a σ-type orbital on NO to the metal, and the second – backdonation from the filled d_{xz} and d_{yz} metal orbitals to the π* orbitals of the NO ligand. Among the MOs of **1** there are no orbitals of pure $\pi_{Re–NO}$ character. The $\pi_{Re–NO}$ bonding interaction makes the largest contribution into HOMO − 2 and HOMO − 1 with α-spin and HOMO − 1, HOMO orbitals with β-spin. A substantial contribution of $\pi_{Re–NO}$ orbitals are also visible in HOMO − 16 and HOMO − 15 with α-spin and HOMO − 15 and HOMO − 12 with β-spin. In

Table 5
The energy and character of the selected occupied molecular orbitals with α- and β-spin for **1** and **2**

	1				**2**			
	α MO		β MO		α MO		β MO	
	E (eV)	Character	*E* (eV)	Character	*E* (eV)	Character	*E* (eV)	Character
HOMO − 19	−9.456	σ_{Cl}, π_{O}, π_{Ph}, π_{pyz}	−9.464	σ_{Cl}, $\sigma_{C–P}$, $\sigma_{C–C}$	−7.832	$\pi_{Cl}(34.3)$, $\pi_{O}(21.4)$, $\pi_{Ph}(25.2)$, $\mathrm{d}_{xz}(10.5) + \pi^{*}_{NO}(5.1)$	−8.202	σ_{Cl}
HOMO − 18	−8.885	$\pi_{Cl}(43.8)$, $\pi_{O}(19.2)$, $\mathrm{d}_{xy}(7.8)$	−9.328	$\pi_{Ph}(50.4)$, $\pi_{O}(21.0)$, $\sigma_{Cl}(8.5)$	−7.706	$\pi_{Ph}(35.4)$, $\pi_{Cl}(26.6)$, $\pi_{O}(12.1)$, $\mathrm{d}_{yz}(14.7) + \pi^{*}_{NO}(9.1)$	−7.772	$\pi_{Cl}(38.5)$, $\pi_{O}(19.5)$, $\mathrm{d}_{yz}(8.7) + \pi^{*}_{NO}(5.7)$
HOMO − 17	−8.709	$\pi_{Cl}(48.4)$, $\pi_{O}(13.7)$, $\mathrm{d}_{xy}(12.3)$	−8.841	$\pi_{Cl}(50.1)$, $\pi_{O}(16.6)$	−7.613	$\pi_{Ph}(41.9)$, $\pi_{Cl}(40.0)$, $\pi_{O}(9.8)$	−7.650	$\pi_{Ph}(55.5)$, $\pi_{Cl}(22.4)$, $\mathrm{d}_{yz}(7.9) + \pi^{*}_{NO}(6.4)$
HOMO − 16	−8.496	$\mathrm{d}_{xz}(32.1) + \pi^{*}_{NO}(16.8)$, $\pi_{Cl}(36.9)$	−8.486	σ_{Cl}, π_{Cl}	−7.527	$\pi_{Ph}(53.5)$, $\pi_{Cl}(37.2)$	−7.579	$\pi_{Cl}(36.7)$, $\pi_{Ph}(36.9)$, $\pi_{O}(12.7)$, $\mathrm{d}_{yz}(5.8) + \pi^{*}_{NO}(5.0)$
HOMO − 15	−8.220	$\pi_{pyz}(37.0)$, $\pi_{Cl}(32.8)$, $\mathrm{d}_{yz}(14.8) + \pi^{*}_{NO}(8.4)$	−8.362	$\mathrm{d}_{xz}(24.1) + \pi^{*}_{NO}(19.1)$, $\pi_{Cl}(47.7)$	−7.475	$\pi_{Ph}(54.6)$, $\pi_{Cl}(33.0)$	−7.496	$\pi_{Ph}(60.5)$, $\pi_{Cl}(33.6)$
HOMO − 14	−8.082	$\sigma_{Cl}(50.1)$, $\pi_{Ph}(19.3)$, $\pi_{O}(11.1)$	−8.168	$\pi_{pyz}(59.4)$, $\pi_{Cl}(25.2)$	−7.421	$\pi_{Ph}(71.2)$, $\pi_{Cl}(15.6)$, $\pi_{O}(8.9)$	−7.418	$\pi_{Ph}(57.1)$, $\pi_{Cl}(27.1)$, $\pi_{O}(6.6)$
HOMO − 13	−8.007	$\pi_{pyz}(30.8)$, $\pi_{Cl}(26.8)$, $\mathrm{d}_{yz}(12.6) + \pi^{*}_{NO}(7.1)$	−7.977	$\pi_{Ph}(69.7)$, $\pi_{Cl}(18.3)$	−7.317	π_{Ph}	−7.406	$\pi_{Ph}(71.0)$, $\pi_{Cl}(20.6)$, $\pi_{O}(4.5)$
HOMO − 12	−7.915	$\pi_{Ph}(60.9)$, $\pi_{Cl}(19.4)$, $\pi_{O}(8.3)$	−7.941	$\pi_{Cl}(41.1)$, $\pi_{pyz}(23.0)$, $\mathrm{d}_{yz}(13.0) + \pi^{*}_{NO}(9.3)$	−7.277	π_{Ph}	−7.295	π_{Ph}
HOMO − 11	−7.752	$\pi_{Ph}(55.6)$, $\pi_{Cl}(29.6)$	−7.860	$\pi_{Cl}(44.6)$, $\pi_{O}(13.7)$	−7.221	$\pi_{Ph}(68.1)$, $\pi_{Cl}(26.8)$	−7.259	π_{Ph}
HOMO − 10	−7.734	n_{pyz}	−7.728	$\pi_{pyz}(44.6)$, $\pi_{Ph}(43.8)$	−7.156	π_{Ph}	−7.158	π_{Ph}
HOMO − 9	−7.703	π_{Ph}	−7.714	$\mathrm{n}_{pyz}(54.4)$, $\pi_{Ph}(35.2)$	−7.073	π_{Ph}	−7.144	π_{Ph}
HOMO − 8	−7.644	π_{Ph}	−7.694	π_{Ph}	−7.013	π_{Ph}	−7.058	π_{Ph}
HOMO − 7	−7.565	$\pi_{Cl}(49.1)$, $\pi_{Ph}(35.7)$	−7.628	π_{Ph}	−6.983	π_{Ph}	−7.004	π_{Ph}
HOMO − 6	−7.564	π_{Ph}	−7.562	π_{Ph}	−6.924	π_{Ph}	−6.951	π_{Ph}
HOMO − 5	−7.489	$\pi_{Cl}(62.9)$, $\pi_{Ph}(29.4)$	−7.535	$\pi_{Cl}(48.5)$, $\pi_{Ph}(33.8)$	−6.918	π_{Ph}	−6.914	π_{Ph}
HOMO − 4	−7.441	$_{Ph}(75.7)$, $\pi_{Cl}(20.0)$	−7.438	$\pi_{Ph}(56.0)$, $\pi_{Cl}(36.1)$	−6.767	$\pi_{Cl}(65.7)$, $\pi_{Ph}(32.0)$	−6.856	$\pi_{Ph}(70.5)$, $\pi_{Cl}(23.5)$
HOMO − 3	−7.094	π_{Cl}	−7.371	π_{Cl}	−6.681	$\pi_{Ph}(54.1)$, $\pi_{Cl}(28.2)$, $\mathrm{n}_{p}.(8.7)$	−6.645	$\pi_{Ph}(42.5)$, $\pi_{Cl}(40.6)$, np.(10.8)
HOMO − 2	−6.573	$\mathrm{d}_{yz}(30.4) + \pi^{*}_{NO}(20.2)$, $\pi_{Cl}(42.8)$	−6.873	π_{Cl}	−6.425	$\mathrm{d}_{yz}(24.9) + \pi^{*}_{NO}(15.4)$, $\pi_{Cl}(44.6)$	−6.569	$\pi_{Cl}(77.7)$, $\pi_{Ph}(19.1)$
HOMO − 1	−6.465	$\mathrm{d}_{xz}(30.3) + \pi^{*}_{NO}(19.6)$, $\pi_{Cl}(48.2)$	−6.462	$\mathrm{d}_{yz}(25.9) + \pi^{*}_{NO}(30.5)$, $\pi_{Cl}(37.2)$	−6.235	$\mathrm{d}_{xz}(30.1) + \pi^{*}_{NO}(22.0)$, $\pi_{Cl}(41.7)$	−6.326	$\mathrm{d}_{yz}(23.3) + \pi^{*}_{NO}(23.1)$, $\pi_{Cl}(39.4)$
HOMO	−5.899	$\mathrm{d}_{xy}(59.1)$, $\pi_{Cl}(34.9)$	−6.361	$\mathrm{d}_{xz}(28.8) + \pi^{*}_{NO}(29.9)$, $\pi_{Cl}(42.6)$	−5.822	$\mathrm{d}_{xy}(53.4)$, $\pi_{Cl}(41.8)$	−6.140	$\mathrm{d}_{xz}(25.1) + \pi^{*}_{NO}(31.8)$, $\pi_{Cl}(38.9)$

Table 6
The energy and character of the selected unoccupied molecular orbitals with α- and β-spin for **1** and **2**

	1				**2**			
	α MO		β MO		α MO		β MO	
	E (eV)	Character	*E* (eV)	Character	*E* (eV)	Character	*E* (eV)	Character
LUMO	−2.322	$\pi^*_{\mathrm{pyz}}(77.8)$, $\pi^*_{\mathrm{NO}}(13.5) - \mathrm{d}_{yz}(2.3)$	−2.909	$\mathrm{d}_{xy}(72.4)$, $\pi_{\mathrm{Cl}}(19.4)$	−1.340	$\mathrm{d}_{x^2-y^2}(22\%) - \sigma_{\mathrm{Cl}}(13.2) - \sigma_{\mathrm{P}}(15.3)$, $\pi^*_{\mathrm{Ph}}(36.3)$	−3.096	$\mathrm{d}_{xy}(65.4)$, $\pi_{\mathrm{Cl}}(25.9)$
LUMO + 1	−1.724	$\pi_{\mathrm{P}}(14.6) + \pi^*_{\mathrm{Ph}}(58.1)$, $\pi^*_{\mathrm{NO}}(6.4) - \mathrm{d}_{yz}(7.9)$	−2.353	$\pi^*_{\mathrm{pyz}}(76.6)$, $\pi^*_{\mathrm{NO}}(13.1) - \mathrm{d}_{yz}(4.2)$	−1.290	$\pi_{\mathrm{P}}(6.6) + \pi^*_{\mathrm{Ph}}(56.7), \mathrm{d}_{x^2-y^2}(11.8)$	−1.296	$\pi_{\mathrm{P}}(12.7) + \pi^*_{\mathrm{Ph}}(72.5)$
LUMO + 2	−1.572	$\pi_{\mathrm{P}}(10.7) + \pi^*_{\mathrm{Ph}}(79.2)$	−1.698	$\pi_{\mathrm{P}}(15.1) + \pi^*_{\mathrm{Ph}}(61.5)$, $\pi^*_{\mathrm{NO}}(5.9) - \mathrm{d}_{yz}(6.6)$	−1.200	$\pi^*_{\mathrm{NO}}(47.7) - \mathrm{d}_{yz}(19.2)$, $\pi^*_{\mathrm{Ph}}(18.6)$	−1.211	$\pi^*_{\mathrm{NO}}(39.2) - \mathrm{d}_{yz}(21.5)$, $\pi^*_{\mathrm{Ph}}(22.9)$
LUMO + 3	−1.336	$\pi^*_{\mathrm{NO}}(30.3) - \mathrm{d}_{xz}(21.2)$, $\pi^*_{\mathrm{Ph}}(29.1)$	−1.570	$\pi_{\mathrm{P}}(10.4) + \pi^*_{\mathrm{Ph}}(80.2)$	−1.102	$\pi^*_{\mathrm{NO}}(45.4) - \mathrm{d}_{xz}(22.5)$, $\pi^*_{\mathrm{Ph}}(18.1)$	−1.175	$\mathrm{d}_{x^2-y^2}(24.0) - \sigma_{\mathrm{Cl}}(15.9) - \sigma_{\mathrm{P}}(16.7)$, $\pi^*_{\mathrm{Ph}}(34.9)$
LUMO + 4	−1.245	$\pi^*_{\mathrm{NO}}(21.4) - \mathrm{d}_{xz}(15.3)$, $\pi^*_{\mathrm{Ph}}(46.7)$	−1.309	$\pi^*_{\mathrm{NO}}(30.6) - \mathrm{d}_{xz}(22.4)$, $\pi^*_{\mathrm{Ph}}(32.0)$	−0.922	π^*_{Ph}	−1.074	$\pi^*_{\mathrm{NO}}(37.9) - \mathrm{d}_{xz}(26.3)$, $\pi^*_{\mathrm{Ph}}(22.1)$
LUMO + 5	−1.130	$\pi^*_{\mathrm{NO}}(29.5) - \mathrm{d}_{yz}(22.3)$, $\pi^*_{\mathrm{Ph}}(25.4)$	−1.225	$\pi^*_{\mathrm{NO}}(13.7) - \mathrm{d}_{xz}(10.4)$, $\pi^*_{\mathrm{Ph}}(63.9)$	−0.876	$\pi_{\mathrm{P}}(7.7) + \pi^*_{\mathrm{Ph}}(82.8)$	−0.909	π^*_{Ph}
LUMO + 6	−1.078	$\mathrm{d}_{x^2-y^2}(29.1) - \sigma_{\mathrm{Cl}}(23.5)$, $\pi^*_{\mathrm{Ph}}(17.9)$, $\pi^*_{\mathrm{pyz}}(17.4)$	−1.066	$\pi^*_{\mathrm{NO}}(29.3) - \mathrm{d}_{yz}(24.8)$, $\pi^*_{\mathrm{Ph}}(22.4)$	−0.845	$\pi_{\mathrm{P}}(7.1) + \pi^*_{\mathrm{Ph}}(68.4)$	−0.872	$\pi_{\mathrm{P}}(8.5) + \pi^*_{\mathrm{Ph}}(85.8)$
LUMO + 7	−1.042	$\pi^*_{\mathrm{pyz}}(68.2)$, $\mathrm{d}_{x^2-y^2}(9.5)$	−1.047	π^*_{pyz}	−0.801	π^*_{Ph}	−0.803	$\pi^*_{\mathrm{Ph}}(68.8)$, $\pi^*_{\mathrm{NO}}(9.4) - \mathrm{d}_{xz}(10.0)$
LUMO + 8	−0.943	π^*_{Ph}	−0.947	$\pi^*_{\mathrm{Ph}}(77.3)$, $\pi^*_{\mathrm{NO}}(7.0) - \mathrm{d}_{yz}(7.1)$	−0.692	π^*_{Ph}	−0.769	$\pi^*_{\mathrm{Ph}}(70.6)$, $\pi^*_{\mathrm{NO}}(4.0) - \mathrm{d}_{yz}(9.3)$
LUMO + 9	−0.793	π^*_{Ph}	−0.836	$\mathrm{d}_{x^2-y^2}(39.7) - \sigma_{\mathrm{Cl}}(33.6)$, $\pi^*_{\mathrm{Ph}}(16.5)$	−0.511	$\mathrm{d}_{z^2}(16.5) - \sigma_{\mathrm{N}}(4.1) - \sigma_{\mathrm{Cl}}(18.2)$, $\pi^*_{\mathrm{Ph}}(79.8)$	−0.687	π^*_{Ph}
LUMO + 10	−0.579	π^*_{Ph}	−0.788	π^*_{Ph}	−0.474	π^*_{Ph}	−0.482	π^*_{Ph}
LUMO + 11	−0.281	$\mathrm{d}_{z^2}(30.5) - \sigma_{\mathrm{Cl}}(20.8)$	−0.580	π^*_{Ph}	−0.265	π^*_{Ph}	−0.353	$\mathrm{d}_{z^2}(21.3) - \sigma_{\mathrm{Cl}}(23.0)$, $\pi^*_{\mathrm{Ph}}(39.3)$

HOMO − 16, HOMO − 2 and HOMO − 1 with α-spin and HOMO − 15, HOMO − 1 and HOMO orbitals with β-spin, the $\pi_{\text{Re–NO}}$ orbitals are mixed with π_{Cl} orbitals. HOMO − 15 with α-spin and HOMO − 12 with β-spin have also a significant contribution of π_{pyz} orbitals. The bonding $\pi_{\text{Re–NO}}$ orbitals with α- and β-spin are localised mainly on the rhenium d orbitals. The anti-bonding $\pi^*_{\text{Re–NO}}$ interaction makes the largest contribution into LUMO, LUMO + 3, LUMO + 4 and LUMO + 5 with α-spin and LUMO, LUMO + 4, LUMO + 5 and LUMO + 6 with β-spin. The $\pi^*_{\text{Re–NO}}$ orbitals have prevalent NO character and they are mixed with π^*_{pyz} or π^*_{Ph} orbitals. Considering the molecular orbital composition and positive total charge on the NO group, the character of the nitrosyl ligand in **1** may be described as NO^+.

The d_{xy} rhenium orbital and π orbitals of the chloride ligands in an anti-bonding arrangement make the main contribution into the HOMO with α-spin and LUMO with β-spin. The LUMO with β-spin is mainly localised on the pyrazine ligand with the admixture of $\pi^*_{\text{Re–NO}}$ anti-bonding orbitals. LUMO + 6 with α-spin and LUMO + 9 with β-spin are mainly of $d_{x^2-y^2} - \sigma_{\text{Cl}} - \sigma_{\text{O}}$ character with a substantial contribution from π^*_{pyz} and π^*_{Ph} orbitals. The dz^2 rhenium orbital is visible in LUMO + 11 with α-spin and LUMO + 12 with β-spin.

3.8. $ReCl_3(NO)(OPPh_3)(PPh_3)]$ (2)

For complex **2**, the π^*_{NO} orbitals are also distributed among several occupied MOs, and the largest contribution of $\pi_{\text{Re–NO}}$ bonding orbitals is noticed for HOMO − 2 and HOMO − 1 with α-spin and HOMO − 1, HOMO orbitals with β-spin. The percent participations of π^*_{NO} orbitals in HOMO − 20 and HOMO − 18 with α-spin and HOMO − 19 and HOMO − 17 with β-spin do not reach 10%. LUMO + 2 and LUMO + 3 with α-spin and LUMO + 2 and LUMO + 4 are mainly composed of $\pi^*_{\text{Re–NO}}$ orbitals (about 60%). Based on the molecular orbital composition and small spin densities on the nitrogen and oxygen atoms of the nitrosyl ligand, the character of the NO group in **2** may be described as NO^+.

Similar to complex **1**, HOMO with α-spin and LUMO with β-spin are d_{xy} rhenium orbitals with the admixture of chlorine π orbitals. The LUMO with α-spin is mainly of $d_{x^2-y^2} - \sigma_{\text{Cl}} - \sigma_{\text{P}}$ character with a substantial contribution from π^*_{Ph} orbitals. The dz^2 rhenium orbital makes a contribution into LUMO + 9 with α-spin and LUMO + 11 with β-spin. HOMO − 3 with α and HOMO − 3 with β-spin are localised on the chloride and phenyl ligands with a substantial contribution from the free electron pair on the phosphorous atom of the PPh_3 molecule.

3.9. NBO analysis

Additional information about the binding in complexes **1** and **2** was obtained by NBO analysis. In open-shell systems, the density operator separates into distinct components for α- and β-spin, leading to the possibility of different NBOs for different spins [54]. Table 7 presents the occupancies and NAO compositions of the selected α- and β-spin NBOs for complexes **1** and **2**. For compound **1**, six natural bond orbitals (three with α-spin and three with β-spin) were detected for the Re–N bond, and two orbitals (one with α-spin and one with β-spin) for the N–O bond. The Re–N bond orbitals of σ-character with α- and β-spins are polarised towards the nitrogen atom (ca. 77% at N) and the s and d orbitals of Re take part in the bonding. The Re–N bond orbitals of π-character are mainly polarised toward the metal atom and only d-orbitals of Re are included in the bonding. The N–O bond orbitals with α- and β-spins are slightly polarised towards the oxygen end. In the valence-bond treatment a linear bonding mode of the nitrosyl group may be represented by the following resonance forms [1]:

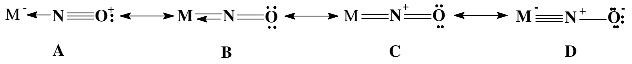

The results of the NBO analysis indicate that the resonance structure of D makes a significant contribution to the structure of complex **1**.

For complex **2**, significantly different NBOs for different spins are observed. One natural bond orbital for the Re–N bond and three orbitals for the N–O bond were detected in the case of orbitals with α-spin, whereas three NBOs for the Re–N bond and one orbital for the N–O bond were detected for orbitals with β-spin. For complex **2**, the α and β natural Lewis structure can be represented by the resonance structure of A and D, respectively. The total occupancy number of the natural bond orbitals for the Re–N bond is larger for complex **1**, whereas the total occupancy number of the NBOs for the N–O bond is larger for **2**. It indicates that the π-backdonation is stronger for complex **1**. The changes of Re–N and N–O bond distances, listed in Tables 1 and 2, also confirm the above-discussed results. An insignificant shortening of the Re–N distance and elongation of the N–O bond length can be noticed for complex **1**.

3.10. Electronic spectra

The experimental and calculated electronic spectra of **1** are presented in Fig. 3. Each calculated transition in Fig. 3(b) was represented by a gaussian function with the height equal to the oscillator strength and width equal to 0.06.

Table 7
Results of the NBO analysis of complexes **1** and **2**

Bond orbital		**1**		**2**	
		α-Spin orbitals	β-Spin orbitals	α-Spin orbitals	β-Spin orbitals
Re–N/BD					
σ	occ.	0.986	0.987	0.982	0.982
	%Re	22.96; sd$^{68.73}$	22.14; sd$^{59.14}$	24.79; sd$^{74.11}$	24.23; sd$^{73.96}$
	%N	77.04; sp$^{37.11}$	77.86; sp$^{36.55}$	75.21; sp$^{37.55}$	75.77; sp$^{40.39}$
π	occ.	0.989	0.991		0.990
	%Re	64.20; d$^{99.92}$	53.43; d$^{99.89}$		52.03; d$^{99.32}$
	%N	35.80; p$^{99.90}$	46.57; p$^{99.92}$		47.97; p$^{99.91}$
π	occ.	0.981	0.998		0.983
	%Re	63.14; d$^{98.93}$	44.82; d$^{99.19}$		52.95; d$^{99.21}$
	%N	36.86; p$^{99.88}$	47.24; p$^{99.91}$		47.07; p$^{95.95}$
N–O/BD					
σ	occ.	0.998	0.998	0.998	0.998
	%N	44.84; sp$^{62.92}$	44.82; sp$^{63.43}$	44.95; sp$^{63.07}$	44.89; sp$^{63.45}$
	%O	55.16; sp$^{68.69}$	55.18; sp$^{68.86}$	55.05; sp$^{68.66}$	55.11; sp$^{68.83}$
π	occ.			0.999	
	%N			33.66; p$^{99.47}$	
	%O			66.34; p$^{99.55}$	
π	occ.			0.999	
	%N			34.05; p$^{99.44}$	
	%O			65.95; p$^{99.59}$	
*Re–N/BD**					
σ	occ.	0.144	0.137	0.178	0.136
π	occ.	0.269	0.226		0.230
π	occ.	0.268	0.226		0.237
*N–O/BD**					
σ	occ.	0.007	0.006	0.006	0.006
π	occ.			0.305	
π	occ.			0.295	

The hybridisation of the atoms is indicated with the percent contribution of the metal-centered d or (and) p orbitals as a superscript.

Tables 8 and 9 show the energy and molar absorption coefficients of the experimental absorption bands and the spin-allowed doublet–doublet electronic transitions calculated with the TDDFT method for **1** and **2**, respectively. The positions and molar absorption coefficients of the electronic bands for complex **2** have been taken from paper [17].

The investigated complexes are of large size and the number of basis functions are equal to 510 and 718 for **1** and **2**, respectively. Eighty electron transitions calculated by the TDDFT method do not comprise all the experimental absorption bands. The UV–Vis spectra of **1** and **2** were calculated to ~260 nm, so the shortest wavelength experimental bands cannot be assigned to the calculated transitions. However, considering that the solution spectra of PPh$_3$, OPPh$_3$ and pyrazine exhibit intense absorption bands in the 260–200 nm region, some additional intraligand and interligand transitions are expected to be found at higher energies in the calculations.

The calculations result in many transitions with very small oscillator strengths. Except for the electronic transitions of $d \rightarrow \pi^*_{NO}$ character and the low energy part of the spectrum, only transitions with oscillator strengths larger than 0.0040 are listed in Tables 7 and 8.

The assignment of the calculated transitions to the experimental bands is based on the criterion of the energy and oscillator strength of the calculated transitions. In the description of the electronic transitions, the main components of the molecular orbital are used. The bonding $\pi_{Re–NO}$ orbitals are assigned as d orbitals, and the antibonding $\pi^*_{Re–NO}$ orbitals as π^*_{NO}.

*3.11. ReCl$_3$(NO)(OPPh$_3$)(pyz)] (**1**)*

In the description of the electronic transitions of **1** the main components of the molecular orbital are used: the LUMO with β-spin is assumed as an orbital of d

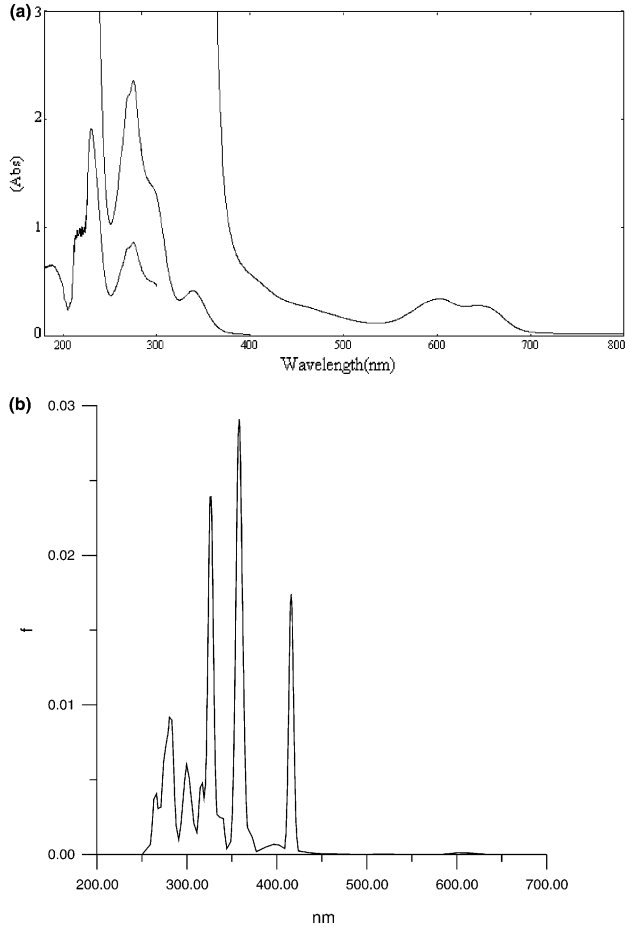

Fig. 3. The experimental (a) and calculated (b) electronic absorption spectrum of **1**.

character, LUMO with α-spin and LUMO + 1 with β-spin are described as π^*_{Ph} orbitals, LUMO + 4 with α-spin and LUMO + 5 with β-spin are treated as π^*_{Ph} orbitals.

The longest wavelength experimental bands at 646.2 and 603.6 nm may be attributed to the transitions of $d_{\mathrm{Re}}/\pi_{\mathrm{Cl}} \rightarrow d$ character with small oscillator strengths, calculated at 621.3 and 600.9 nm, respectively.

The weak absorption band at 458.9 nm is assigned to the calculated transitions with small oscillator strengths at 526.4 and 463.2 nm. The first one corresponds mainly to the electronic transition from the rhenium d orbitals onto π* orbitals of the nitrosyl group. Considering that the bonding $\pi_{\mathrm{Re-NO}}$ and anti-bonding $\pi^*_{\mathrm{Re-NO}}$ orbitals are mixed with the π chloride and π^*_{Ph} orbitals respectively, the character of the transition at 526.4 nm is determined as $d_{\mathrm{Re}}/\pi_{\mathrm{Cl}} \rightarrow \pi^*_{\mathrm{NO}}/\pi^*_{\mathrm{Ph}}$. The transition at 463.2 nm is of $d_{\mathrm{Re}}/\pi_{\mathrm{Cl}} \rightarrow \pi^*_{\mathrm{pyz}}$ origin.

The experimental band at 408.5 nm is also attributed to transitions of $d/\pi_{\mathrm{Cl}} \rightarrow \pi^*_{\mathrm{Ph}}$ and $d/\pi_{\mathrm{Cl}} \rightarrow d/\pi^*_{\mathrm{Ph}}/\pi^*_{\mathrm{pyz}}$ character with small oscillator strengths, calculated at 449.0 and 437.3 nm, respectively.

The experimental absorption band at 359.4 nm is assigned to the transition calculated between 420 and 335 nm. These transitions are mainly of LMCT ($\pi_{\mathrm{Cl}} \rightarrow d$) character. The electronic transitions from the rhenium d orbitals onto π* orbitals of the nitrosyl group calculated in the range 420–335 nm have small oscillator strengths and they do not contribute significantly to the overall shape of the spectrum.

The experimental band at 309.0 nm is attributed to the calculated transition of $\pi_{\mathrm{Cl}} \rightarrow \pi^*_{\mathrm{pyz}}$ character at 326.7 nm and some LMCT ($\pi_{\mathrm{Cl}}/\pi_{\mathrm{Ph}}/\pi_{\mathrm{O}} \rightarrow d$) transitions. LUMO + 1 with β-spin has a substantial admixture of the rhenium d orbitals, so the transition from chloride ligand to π^*_{pyz} orbitals are mediated by the metal.

*3.12. ReCl$_3$(NO)(OPPh$_3$)(PPh$_3$)] (**2**)*

In the description of the electronic transitions of **2** the main components of the molecular orbital are used: the LUMO with β-spin is assumed as an orbital of d character. LUMO + 1 and LUMO + 2 with α-spin and LUMO + 2 and LUMO + 4 with β-spin are described as π^*_{NO} orbitals.

The longest wavelength experimental bands at 719.9 and 656.2 nm may be attributed to transitions of $d/\pi(\mathrm{Cl}) \rightarrow d$ character with small oscillator strengths, calculated at 756.8 and 671.3 nm, respectively.

The experimental absorption bands at 421.0 and 356.0 nm are assigned to the LMCT ($\pi_{\mathrm{Cl}} \rightarrow d$, $\pi_{\mathrm{Ph}} \rightarrow d$ and $n(P) \rightarrow d$) transitions with large oscillator strengths. In comparison with complex **1**, the LMCT ($\pi_{\mathrm{Cl}} \rightarrow d$, $\pi_{\mathrm{Ph}} \rightarrow d$ and $n(P) \rightarrow d$) electronic transitions are bathochromically shifted. The electronic transitions from the rhenium d orbitals onto π* orbitals of the nitrosyl group have small oscillator strengths and they do not contribute significantly to the overall shape of the bands at 421.0 and 356.0 nm. Similar to complex **1**, they are hidden under the more intense transitions of LMCT character. However, such small values of the oscillator strengths seem to be typical of $d \rightarrow \pi^*_{\mathrm{NO}}$ transitions, and they have been supported by the calculations for other metal nitrosyls [55,56].

The experimental band at 279.0 is mainly attributed to the calculated transition of $\pi_{\mathrm{Cl}} \rightarrow d$ character at 298.5 nm.

The intense absorption band at 266.0 is assigned to the interligand charge transfer transitions, but this assignment is probably not complete. Similar to complex **1**, some additional intraligand and interligand transitions can be expected at higher energies in the calculated spectrum.

Table 8
The energy and molar absorption coefficients of the experimental absorption bands and the electronic transitions calculated with the TDDFT method for **1**

The most important orbital excitations	Character	λ (nm)	E (eV)	f	Experimental, Λ [nm] (E [eV]) ε
H(β) → L(β)	d$_{xz}$/π(Cl) → d$_{xy}$	621.3	2.00	0.0002	646.2 (1.92) 50
H − 1(β) → L(β)	d$_{yz}$/π(Cl) → d$_{xy}$	600.9	2.06	0.0001	603.6 (2.05) 60
H − 1(α) → L + 3(α)	d$_{xz}$/π(Cl) → π*(NO)/π*(Ph)	526.4	2.36	0.0002	458.9 (2.70) 30
H(β) → L + 4(β)	d$_{xz}$/π(Cl) → π*(NO)/π*(Ph)				
H − 1(β) → L + 6(β)	d$_{yz}$/π(Cl) → π*(NO)/π*(Ph)				
H(α) → L(α)	d$_{xy}$/π(Cl) → π*(pyz)	463.2	2.68	0.0002	
H(α) → L + 1(α)	d$_{xy}$/(Cl) → π*(Ph)	449.0	2.76	0.0001	408.5 (3.04) 70
H(α) → L + 6(α)	d$_{xy}$/π(Cl) → d$_{x^2-y^2}$/π*(Ph)/π*(pyz)				
H(β) → L + 4(β)	d$_{xz}$/π(Cl) → π*(NO)/π*(Ph)	437.3	2.84	0.0001	
H − 1(β) → L + 1(β)	d$_{yz}$/π(Cl) → π*(pyz)				
H − 2(β) → L(β)	π(Cl) → d$_{xy}$	416.1	2.98	0.0175	359.4 (3.45) 1040
H(α) → L + 3(α)	d$_{xy}$/π(Cl) → π*(NO)/π*(Ph)	399.4	3.10	0.0011	
H − 2(α) → L(α)	d$_{yz}$/π(Cl) → π*(pyz)	362.4	3.42	0.0080	
H(α) → L + 5(α)	d$_{xy}$/π(Cl) → π*(NO)/π*(Ph)	358.8	3.45	0.0045	
H − 3(β) → L(β)	π(Cl) → d$_{xy}$	357.9	3.46	0.0204	
H − 5(β) → L(β)	π(Cl)/π(Ph) → d$_{xy}$	354.4	3.50	0.0061	
H − 2(α) → L + 3(α)	d$_{yz}$/π(Cl) → π*(NO)/π*(Ph)	339.4	3.65	0.0016	
H − 1(β) → L + 4(β)	d$_{yz}$/π(Cl) → π*(NO)/π*(Ph)				
H − 2(β) → L + 1(β)	π(Cl) → π*(pyz)	326.7	3.79	0.0143	309.0 (4.01) 3850
H − 11(β) → L(β)	(Cl)/π(O) → d$_{xy}$				
H(α) → L + 2(α)	d$_{xy}$/π(Cl) → π*(Ph)	324.7	3.82	0.0042	
H(α) → L + 11(α)	d$_{xy}$/π(Cl) → d$_{z^2}$	316.2	3.92	0.0049	
H − 116(β) → L(β)	σ(Cl)/π(Cl) → d$_{xy}$	282.8	4.43	0.0045	
					275.4 (4.51) 9890
					230.4 (5.38) 22000

ε, Molar absorption coefficient (dm^3 mol^{-1} cm^{-1}).

Table 9
The energy and molar absorption coefficients of the experimental absorption bands and the electronic transitions calculated with the TDDFT method for **1**

The most important orbital excitations	Character	λ (nm)	E (eV)	f	Experimental, Λ [nm] (E [eV]) ε
H(β) → L(β)	d$_{xz}$/π(Cl) → d$_{xy}$	756.8	1.64	0.0001	719.9 (1.72) 17
H − 1(β) → L(β)	d$_{yz}$/π(Cl) → d$_{xy}$	671.3	1.85	0.0002	656.2 (1.89) 40
H − 1(α) → L + 3(α)	d$_{xz}$/π(Cl) → π*(NO)	497.3	2.49	0.0002	421.0 (2.94) 2100
H − 2(β) → L(β)	π(Cl)/π(Ph) → d$_{xy}$	485.9	2.55	0.0093	
H − 3(β) → L(β)	π(Ph)/π(Cl)/n(P) → d$_{xy}$	469.5	2.64	0.0198	
H(α) → L(α)	d$_{xy}$/π(Cl) → d$_{x^2-y^2}$/π*(Ph)	426.2	2.91	0.0011	
H(β) → L + 2(β)	d$_{xz}$/π(Cl) → π*(NO)	415.5	2.98	0.0001	
H − 4(β) → L(β)	π(Ph)/π(Cl) → d$_{xy}$	413.2	3.00	0.0103	
H − 1(β) → L + 2(β)	d$_{yz}$/π(Cl) → π*(NO)	404.0	3.07	0.0002	356.0 (3.48) 1793
H − 5(β) → L(β)	π(Ph) → d$_{xy}$	403.1	3.08	0.0022	
H − 6(β) → L(β)	π(Ph) → d$_{xy}$	383.1	3.24	0.0046	
H(α) → L + 2(α)	d$_{xy}$/π(Cl) → π*(NO)	371.6	3.34	0.0009	
H(α) → L + 3(α)	d$_{xy}$/π(Cl) → π*(NO)	366.1	3.39	0.0015	
H − 1(α) → L + 2(α)	d$_{xz}$/π(Cl) → π*(NO)	352.7	3.51	0.0001	
H(β) → L + 2(β)	d$_{xz}$/π(Cl) → π*(NO)				
H − 2(α) → L + 2(α)	d$_{yz}$/π(Cl) → π*(NO)	315.2	3.93	0.0004	
H − 1(α) → L + 3(α)	d$_{xz}$/π(Cl) → π*(NO)				
H − 2(α) → L + 3(α)	d$_{yz}$/π(Cl) → π*(NO)	308.6	4.02	0.0002	
H − 21(β) → L(β)	π(Cl) → d$_{xy}$	298.5	4.15	0.0206	279.0 (4.44) 7 811
H − 2(α) → L + 3(α)	d$_{yz}$/π(Cl) → π*(NO)	298.1	4.16	0.0057	
H − 2(β) → L + 3(β)	π(Cl)/π(Ph) → d$_{x^2-y^2}$/π*(Ph)	268.2	4.62	0.0071	266.0(4.66)15 800
H − 3(α) → L + 2(α)	π(Ph)/π(Cl)/n(P) → π*(NO)/π*(Ph)	265.5	4.67	0.0134	
H − 4(α) → L + 2(α)	π(Cl)/π(Ph) → π*(NO)	261.2	4.75	0.0050	

ε, Molar absorption coefficient (dm^3 mol^{-1} cm^{-1}).

4. Conclusions

The $[ReCl_3(NO)(OPPh_3)(pyz)]$ (**1**) complex has been obtained by two different routes, and characterised by IR, UV–Vis and magnetic measurements. Its crystal and molecular structure has been determined. Theoretical studies of $[ReCl_3(NO)(OPPh_3)(pyz)]$ and the related complex $[ReCl_3(NO)(OPPh_3)(PPh_3)]$ (**2**) have been performed by the DFT method with the aim to investigate their molecular and electronic structures, spectral properties and bonding. Most of the MOs of **1** and **2** have complicated character. The electronic configuration of the metal center in the investigated complexes is as follows: $(d_{xz})^2(d_{yz})^2(d_{xy})^1$. The d_{xy} rhenium orbital makes the main contributions into the HOMO with α-spin and LUMO with β-spin. The occupied d_{yz} and d_{xz} rhenium orbitals participate in back-donation from the central ion to the NO ligand. However, the d_{yz}/d_{xz} and π^*_{NO} orbitals are distributed among several occupied MOs to give a considerable contribution into several HOMO and LUMO orbitals. For both complexes, the bonding π_{Re-NO} orbitals are localised mainly on the rhenium d orbitals, whereas the π^*_{Re-NO} orbitals have prevalent NO character. The results of the NBO analyses indicate a stronger π-backdonation in complex **1**. A shortening of the Re–N distance and elongation of the N–O bond length observed for complex **1** confirms it. The TDDFT calculations for complexes **1** and **2** reveal that the electronic transitions from the rhenium d orbitals onto the π* orbitals of the nitrosyl group have small oscillator strengths and they do not contribute significantly to the overall shape of the spectrum. They are hidden under the more intense transitions of LMCT character.

5. Supplementary data

Supplementary data for $C_{22}H_{19}Cl_3N_3O_2PRe$ are available from the CCDC, 12 Union Road, Cambridge CB2 1EZ, UK (fax: +44 1223 336033; e-mail: deposit@ccdc.cam.ac.uk or at www: http://www.ccdc.cam.ac.uk) on request, quoting the deposition number: 243040.

Acknowledgements

The GAUSSIAN03 calculations were carried out in the Wrocław Centre for Networking and Supercomputing, WCSS, Wrocław, Poland under calculational Grant No. 51/96.

References

[1] G.B. Richter-Addo, P. Legzdins, Metal Nitrosyls, Oxford University Press, Oxford, 1992.

[2] J.A. McCleverty, Chem. Rev. 79 (1979) 53.

[3] J.N. Kukuškin, Reakcionnaja sposobnost koordinacjonnych soedinienij, Chimija, Leningrad, 1987.

[4] J.H. Enemark, R.D. Feltham, Coord. Chem. Rev. 13 (1974) 339.

[5] K.G. Caulton, Coord. Chem. Rev. 14 (1975) 317.

[6] F. Bottomley, Coord. Chem. Rev. 26 (1978) 7.

[7] K.K. Pandey, Coord. Chem. Rev. 51 (1983) 70.

[8] G. Wilkinson, Comprehensive Coordination Chemistry, vol. 2, Pergamon Press, Oxford, 1987, p. 100.

[9] G.B. Richter-Addo, P. Legzdins, J. Burstyn, Chem. Rev. 102 (2002) 857.

[10] T.W. Hayton, P. Legzdins, W.B. Sharp, Chem. Rev. 102 (2002) 935.

[11] J.A. McCleverty, Chem. Rev. 104 (2004) 403.

[12] W. Volkert, W.F. Goeckeler, G.J. Ehrhardt, A.R. Ketring, J. Nucl. Med. 32 (1991) 174.

[13] E.A. Deutsch, K. Libson, J.L. Vanderheyden, Technetium and Rhenium in Chemistry and Nuclear Medicine, Raven Press, New York, 1990.

[14] J.O. Dzięgielewski, B. Machura, J. Marek, Polyhedron 15 (1996) 3713.

[15] J.O. Dzięgielewski, B. Machura, T.J. Bartczak, Polyhedron 15 (1996) 2813.

[16] T.J. Bartczak, W. Czurak, J.O. Dzięgielewski, B. Machura, Polish J. Chem. 72 (1998) 633.

[17] J.O. Dzięgielewski, B. Machura, T. Kupka, T.J. Bartczak, W. Czurak, Polish J. Chem. 72 (1998) 1009.

[18] J.O. Dzięgielewski, B. Machura, T.J. Bartczak, W. Czurak, J. Kusz, J. Warczewski, J. Coord. Chem. 48 (1999) 125.

[19] T.J. Bartczak, W. Czurak, J.O. Dzięgielewski, B. Machura, A. Jankowska, J. Kusz, J. Warczewski, Polyhedron 18 (1999) 2313.

[20] T.J. Bartczak, W. Czurak, J.O. Dzięgielewski, B. Machura, J. Kusz, J. Warczewski, Polish J. Chem. 74 (2000) 265.

[21] T.J. Bartczak, W. Czurak, J.O. Dzięgielewski, B. Machura, A. Jankowska, J. Kusz, J. Warczewski, J. Coord. Chem. 52 (2001) 361.

[22] B. Machura, J.O. Dzięgielewski, S. Michalik, T.J. Bartczak, R. Kruszynski, J. Kusz, Poyhedron 21 (2002) 2617.

[23] M.C. Aragoni, M. Arca, T. Cassano, C. Denotti, F.A. Devillanova, F. Isaia, V. Lippolis, D. Natali, L. Niti, M. Sampietro, R. Tommasi, G. Verani, Inorg. Chem. Commun. 5 (2002) 869.

[24] P. Romaniello, F. Lelj, Chem. Phys. Lett. 372 (2003) 51.

[25] P. Norman, P. Cronstrand, J. Ericsson, Chem. Phys. 285 (2002) 207.

[26] J. Bossert, N.B. Amor, A. Strich, C. Daniel, Chem. Phys. Lett. 342 (2001) 617.

[27] C.E. Powell, M.P. Cifuentes, A.M. McDonagh, S.K. Hurst, N.T. Lucas, C.D. Delfs, R. Stranger, M.G. Humphrey, S. Houbrechts, I. Asselberghs, A. Persoons, D.C.R. Hockless, Inorg. Chim. Acta 352 (2003) 9.

[28] J.P. Morral, C.E. Powell, R. Stranger, M.P. Cifuentes, M.G. Humphrey, G.A. Heath, J. Organomet. Chem. 670 (2003) 248.

[29] P. Romaniello, F. Lelj, J. Mol. Struct. Theochem. 636 (2003) 23.

[30] A. Voigt, U. Abram, R. Böttcher, U. Richter, J. Reinhold, R. Kirmse, Chem. Phys. 253 (2000) 171.

[31] M. Lipowska, L. Hansen, R. Cini, X. Xu, H. Choi, A.T. Taylor, L.G. Marzilli, Inorg. Chim. Acta 339 (2002) 327.

[32] J. Gancheff, C. Kremer, E. Kremer, O.N. Ventura, J. Mol. Struct. (Theochem) 580 (2002) 107.

[33] M.L. Kuznestov, E.A. Klestova-Nadeeva, A.I. Dement'ev, J. Mol. Struct. (Theochem) 671 (2004) 229.

[34] N. Psaroudakis, K. Mertis, D.G. Liakos, E.D. Simandiras, Chem. Phys. Lett. 369 (2003) 490.

[35] X.-Y. Liu, S. Bouherour, H. Jacobsen, H.W. Schmalle, H. Berke, Inorg. Chim. Acta 330 (2002) 250.

[36] É. Bencze, J. Mink, I. Pápai, I.S. Butler, D. Lafleur, D.F.R. Gilson, J. Organomet. Chem. 616 (2000) 1.

[37] W.-Y. Wong, S.-H. Cheung, X. Huang, Z. Lin, J. Organomet. Chem. 655 (2002) 39.

[38] G. Rouschias, G. Wilkinson, J. Chem. Soc. A (1966) 465.

[39] STOE & Cie (1999), X-RED, Version 1.18, STOE & Cie GmbH, Darmstadt, Germany.

[40] G.M. Sheldrick, Acta Crystallogr. A 46 (1990) 467.

[41] G.M. Sheldrick, SHELXL97. Program for the Solution and Refinement of Crystal Structures, University of Göttingen, Germany, 1997.

[42] G.M. Sheldrick, SHELXTL: Release 4.1 for Siemens Crystallographic Research Systems, 1990.

[43] M.J. Frisch, G.W. Trucks, H.B. Schlegel, G.E. Scuseria, M.A. Robb, J.R. Cheeseman, J.A. Montgomery Jr., T. Vreven, K.N. Kudin, J.C. Burant, J.M. Millam, S.S. Iyengar, J. Tomasi, V. Barone, B. Mennucci, M. Cossi, G. Scalmani, N. Rega, G.A. Petersson, H. Nakatsuji, M. Hada, M. Ehara, K. Toyota, R. Fukuda, J. Hasegawa, M. Ishida, T. Nakajima, Y. Honda, O. Kitao, H. Nakai, M. Klene, X. Li, J.E. Knox, H.P. Hratchian, J.B. Cross, C. Adamo, J. Jaramillo, R. Gomperts, R.E. Stratmann, O. Yazyev, A.J. Austin, R. Cammi, C. Pomelli, J.W. Ochterski, P.Y. Ayala, K. Morokuma, G.A. Voth, P. Salvador, J.J. Dannenberg, V.G. Zakrzewski, S. Dapprich, A.D. Daniels, M.C. Strain, O. Farkas, D.K. Malick, A.D. Rabuck, K. Raghavachari, J.B. Foresman, J.V. Ortiz, Q. Cui, A.G. Baboul, S. Clifford, J. Cioslowski, B.B. Stefanov, G. Liu, A. Liashenko, P. Piskorz, I. Komaromi, R.L. Martin, D.J. Fox, T. Keith, M.A. Al-Laham, C.Y. Peng, A. Nanayakkara, M. Challacombe, P.M.W. Gill, B. Johnson, W. Chen, M.W. Wong, C. Gonzalez, J.A. Pople, GAUSSIAN03, Revision B.03, Gaussian Inc., Pittsburgh, PA, 2003.

[44] A.D. Becke, J. Chem. Phys. 98 (1993) 5648.

[45] C. Lee, W. Yang, R.G. Parr, Phys. Rev. B 37 (1988) 785.

[46] M.E. Casida, in: J.M. Seminario (Ed.), Recent Developments and Applications in Modern Density Functional Theory, Theoretical and Computational Chemistry, vol. 4, Elsevier, Amsterdam, 1996.

[47] P.J. Hay, W.R. Wadt, J. Chem. Phys. 82 (1985) 299.

[48] E.D. Glendening, A.E. Reed, J.E. Carpenter, F. Weinhold, NBO (version 3.1).

[49] G.A. Jeffrey, W. Saenger, Hydrogen Bonding in Biological Structures, Springer-Verlag, New York, 1994.

[50] G.R. Desiraju, T. Steiner, The Weak Hydrogen Bond in Structural Chemistry and Biology, Oxford University Press, Oxford, 1999.

[51] E. Iengo, E. Zangrando, S. Mestroni, G. Fronzoni, M. Stener, E. Alessio, J. Chem. Soc., Dalton Trans. (2001) 1338.

[52] B.L. Haymore, I.A. Ibers, Inorg. Chem. 14 (1975) 3060.

[53] J.P. Collman, J.T. McDevitt, C.R. Leinder, G.T. Yee, J.B. Torrance, W.A. Little, J. Am. Chem. Soc. 109 (1987) 4606.

[54] A.E. Reed, L.A. Curtiss, F. Weinhold, Chem. Rev. 88 (1988) 899.

[55] S.C. da Silva, D.W. Franco, Spectrochim. Acta 55A (1999) 1515.

[56] S.I. Gorelsky, S.C. da Silva, A.B.P. Lever, D.W. Franco, Inorg. Chim. Acta 300–302 (2000) 698.